Electron paramagnetic resonance approaches to study biologically relevant reactions: examples from amyloid aggregation to enzymes

Passerini, L.

Chapter 5.
Pulsed Electron Paramagnetic Resonance on Cu(II)-Cage Compounds With Respectively Six or Eight Copper Ions

A publication of the work described in this chapter is in preparation: L. Passerini, E.O. Bobylev, F.J. de Zwart, H. Hintz, A. Godt, B. de Bruin, J.N.H. Reek and M. Huber ”Pulsed electron paramagnetic resonance on Cu(II) cage compounds with six, respectively eigth copper ions”, to be submitted.

5.1 Introduction

Complexes in which more than two units interact at nano-meter distances to generate function are important in many areas from biology to chemistry. Examples are multimeric protein (sub-) units in biochemistry [1-4] or multiple (transition) metal-ion centers in molecular catalysts [1, 5, 6]. For the latter, there has recently been a surge of interest in radical-based supramolecular systems, owing to their diverse properties and promising applications [8]. The presence of multiple spins within a confined spatial arrangement and a defined geometric structure in such systems gives rise to adjustable spin-spin interactions [10-12]. Moreover, encapsulation of paramagnetic guest molecules creates promising candidates for sensor materials [8, 10-12]. The integration of radicals and metal ions into supramolecular architectures also gives them redox properties for potential catalytic applications [6-8]. In the past, the analysis of radical-based supramolecular systems predominantly relied on continuous wave electron paramagnetic resonance (EPR) techniques [10-12]. Pulsed EPR adds the possibility of obtaining structural information, and in particular, pulsed dipolar EPR spectroscopy that provides nano-meter distance constraints is promising. Methods, such as double electron-electron resonance (DEER or PELDOR) have proven their value in many areas of chemistry and biology [13-17]. While the theory and practice of the investigation of two-spin systems, i.e. the interaction between pairs of spins, is established, as reviewed in [18, 19], cases where more than two spins interact within a nano-object still present challenges.

If more than two spins interact in the DEER sensitive distance range, the modulation depth becomes larger than in two-spin systems. For a two-spin system, the modulation depth is given by the inversion efficiency λ, whereas for multispin systems the modulation depth Δ is given by equation:

$$\Delta_N = 1 - (1 - \lambda)^{N-1} \qquad (1)$$

where N is the number of interacting spins [20]. This increase in modulation depth was used as a method for counting monomers in nanoobjects, first by Tsvetkov et al. [21, 22], in oligomers of biological systems [20, 23-25]. Additionally, ghost peaks in the distance distributions can occur. These peaks do not represent actual distances, but derive from sum- and difference-frequencies of the dipolar frequencies measured by DEER [26]. Such ghost peaks can obscure the pair-wise distances and thereby interfere with using DEER distances for structural information. Approaches proposed to identify and suppress ghost peaks are proposed in literature [26-29]. Among those, adjustment of inversion efficiency is the most common method that can be used during data acquisition, by reducing the power of the pump-pulse. Also, see von Hagens et al. [26], power scaling in processing the data is possible. This method is commonly known as “ghost suppression”, as it suppresses the ghost distances [26]. On systems containing up to eight nitroxides Valera et al. [28] showed

that while power scaling or reduction of the inversion efficiency alone are not enough, a combination of the two still allows for reliable extraction of spin-pair distances, even though the expected relative intensities of the distance peaks were not recovered [28]. Considering metal ions, there is only one study, by Edwards et al. [30], where DEER experiments were performed on a labelled proteorhodopsin hexamer, comparing nitroxide and Gd(III) based spin labels. Multispin effects in the Gd(III) labelled samples were strongly reduced with respect to nitroxides, an effect that was attributed to the naturally low inversion efficiency for Gd(III) [30].

Here we investigate multi-spin interactions in the copper(II) cages Pd12Cu6 ($Pd_{12}Cu_6L^{DMAP}_{24}$)(**Cu6**) and Pd12Cu8 ($Pd_{12}Cu_8L^{Pro}_{24}$) (**Cu8**) (fig.1), with respectively six and eight copper(II) ions. The synthesis, structural characterization and catalytic interest in these systems were described in [7]. The regular geometric structure of the copper cages and the presence of a relatively large number of Cu(II) ions in a defined arrangement make them particularly attractive, in particular, since multispin effects systems with large magnetic anisotropy are limited so far (see above) [26, 27]. Therefore, the copper cages **Cu6** and **Cu8** present an ideal system to test multi-spin effects in Cu(II) systems. It has to be noted that the Cu(II)-derivatives of the cage molecules investigated here are not as stable as the term "model compounds" may imply. Prolonged handling at room temperature causes decay, and the Cu(II) centers have a tendency to reduce to Cu(I) making them EPR inactive [7].

In the present study, the application of 9 GHz DEER on the multi-copper cages shown in figure 1 is described, revealing multispin interactions, i.e. the interaction of more than two spins. The distances confirm that for **Cu6** the structure shown in figure 1B applies. For **Cu8,** the model shown in fig.1A is consistent with the DEER data.

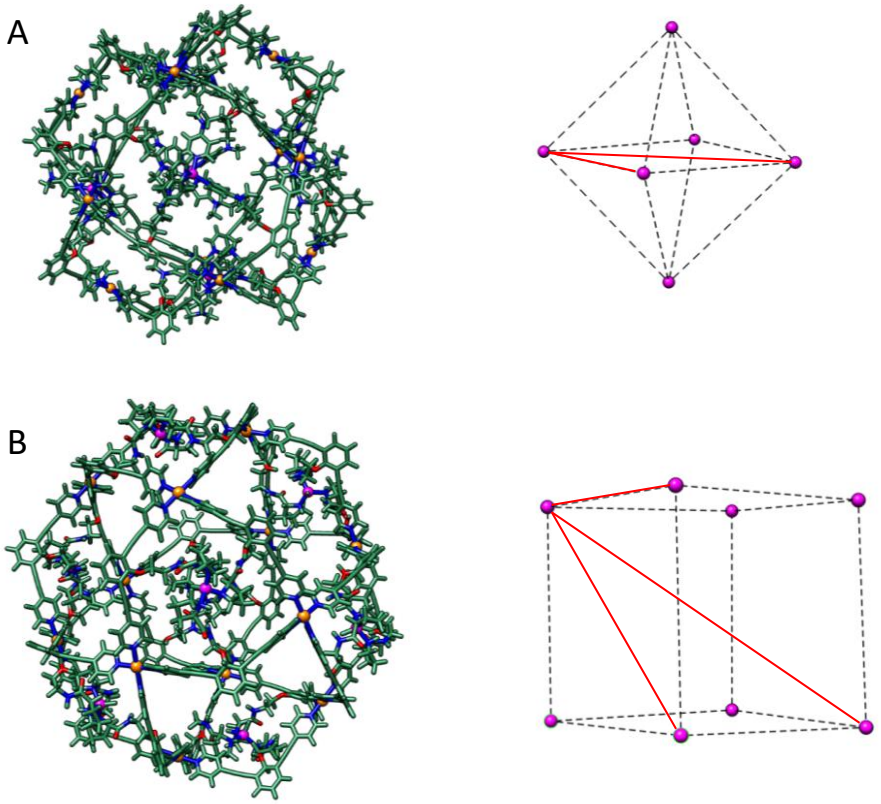

Figure 1. Structures of the Cu(II) cages studied in this work (left), and sketch of the spatial arrangement of the coordinated copper ions (right). A) **Cu6**. The copper ions are located in the six square windows of the nanosphere, forming an octahedron, giving a total of 2 different distances, highlighted in red. B) **Cu8**. The copper ions are located in the triangular windows of the nanosphere, forming a cube, giving a total of three different distances. Magenta spheres: copper ions, yellow spheres: palladium ions, green: functional groups coordinating the copper ion, red lines: highlight of the different copper distances inside the cages. For details, see [7].

5.2 Materials and Methods

EPR spectroscopy

Pulsed EPR measurements were performed at 9 GHz on an Elexsys E680 spectrometer (Bruker) using a 3 mm ER 4118 X-MD-3-W1 split-ring resonator. The cryogenic temperature of 20K was obtained with helium gas in a CF935 (Oxford Instruments) cryostat with an ITC502 temperature controller (Oxford Instruments). Samples were prepared in 3 mm outer-diameter quartz tubes, frozen and stored in liquid nitrogen before insertion into the precooled helium gas-flow cryostat.

The four-pulse DEER [4, 5] sequence $(\pi/2)_1$-τ_1- $(\pi)_1$–$(\tau_1 + t)$-$(\pi)_2$–$(\tau_2$-$t)$-$(\pi)_1$–τ_2-[echo] was employed, where subscripts 1 and 2 indicate events occurring at the observer and pump frequency, respectively. The pump and observer frequencies were separated by 75 MHz. The power of the pump pulse was adjusted to invert the echo maximally. The lengths of the pulses at the observer frequency were 16 and 32 ns for the π /2 and π pulses, respectively. The length of the pump pulse was 16 ns. In the measurements, the τ time was incremented with 8 ns steps starting at τ = 140 ns to suppress nuclear modulation. The slices were added to obtain hyperfine-modulation-free time traces and phase corrected. Regular traces were measured with a total evolution time of 2152 ns. For modulation- depth comparison, a separate experiment with shorter evolution time and a back-to-back measurement of **Cu6**, **Cu8** and **Cu2** was performed.

The DEER data were analyzed using the DeerAnalysis2019 and DeerAnalysis2023 programs [31], which are available from http://www.epr.ethz.ch/ software/index. DeerAnalysis2019 version was used for Tikhonov regularization and gaussian fitting, while DeerAnalysis2023 ws used for DEERNet analysis. Contribution of a known instrumentation artifact at 1940 ns could not be completely eliminated from the real part, therefore all traces were truncated to 1932 ns. Zero time of the traces was 88 ns. After background correction of the data using a three-dimensional background, the distance distribution was determined by Tikhonov regularization, with a regularization parameter of 125. Validation was performed using the validation tool in DeerAnalysis. For **Cu6** the white-noise contribution was varied between 0.02 and 1.5 with 10 steps, and the background start from 372 ns to 1000 ns with 20 steps. For **Cu8** the white-noise contribution was varied between 0.03 and 1.5 with 10 steps, and the background start from 372 ns to 1000 ns with 20 steps. The shaded areas in the distance distribution plots show, for a given distance, the lower and upper error bounds (two times the standard deviation) calculated over all the validation steps.

Sample preparation

Cu6 and **Cu8** were synthesized as described in [7]. **Cu2** was synthesized as described in [9]. Samples: **Cu6** and **Cu8**: solvent: 3 : 1 butylnitrile : acetonitrile, copper concentration 0.63 mM (**Cu6**) and 0.83 mM (**Cu8**). **Cu2** solvent: 50% v/v glycerol : water solution, concentration 0.6 mM

5.3 Results

In this study DEER data were acquired by 9 GHz EPR spectroscopy on the **Cu8** and **Cu6** cages. A two-copper complex (**Cu2**), structure see figure SI2, was used as reference [9]. In the following, we present the outcome of the characterization.

The DEER traces obtained for **Cu8** and **Cu6** are shown in figure 2A. The length of the traces is 2 µs, a length that is similar to the DEER evolution time obtained in similar experiments on Cu(II)-pairs in the literature [32-34]. The traces of **Cu8** and **Cu6** are clearly different from one another. Both show an initial fast decay, which suggests the presence of short distances. In **Cu6**, there is a clear modulation maximum around 450 ns, while for **Cu8** there are no clear oscillations. The difference between the two traces is even more evident in figure 2B, where the traces are shown after background subtraction.

In figure 2C and 2D the distance distributions are shown. They are obtained considering only spin-pair contributions. For **Cu6** (figure 2C) two distinct distance peaks are observed, one is centered around 1.8 nm , and a second peak with approximately the same intensity is centered around 2.6 nm (see Table 1). A peak with a small population around 3.6 nm is seen, but validation shows that this peak is not reliable. The sample **Cu8** (figure 2D) also shows two distance peaks, at roughly similar distances, yet the peak centered at 1.8 nm is broader, respectively, and a shoulder around 2 nm can be discerned, also the intensity is larger than the one of the peak around 2.8 nm. A peak with a small population around 3.8 nm is seen, but validation shows that this peak is not reliable. All relevant distances are given in table 1. The distance peaks obtained for **Cu6** are narrower than the ones obtained for **Cu8**. In general, the width of the distance peaks is maximally 0.2 nm full width at half maximum (FWHM), in line with spin pairs in other rigid copper systems reported in the literature [9].

Since modulation depth strongly depends on experimental conditions, **Cu2** [9] was used as a reference compound. It contains two Cu(II) ions at a distance of 3.3 nm. The DEER properties of this reference sample agree with those measured before [9]. In figure 3, the DEER trace of **Cu2** (green trace) is shown alongside the DEER traces of **Cu6** and **Cu8**. The modulation depth is 23 % for **Cu6**, 22 % for **Cu8**, and 13 % for **Cu2**. Higher modulation depth is associated with multispin effects, revealing that the **Cu6** and **Cu8** DEER traces show

interactions between more than two Cu(II) ions. Quantitatively, equation 1 gives the relation between the number of interacting electron spins N and the modulation depth. For the cages, this relation shows interaction of approximately three spins, a number we will discuss in detail below.

Interaction of multiple spins with distances in the DEER sensitive range not only affects the modulation depth, but can also give rise to sum- and difference-frequencies that can manifest themselves as extra peaks in the distance distribution, so called ghost peaks. In figure 4, the effects of the application of the ghost suppression tool in DeerAnalysis, see Materials and methods, on the distance distributions are shown for three interacting spins. Similar effects are seen for higher numbers of spins, see figure SI5 and SI6 in the SI. The changes in the distance distribution upon ghost suppression (figure 4) are small, and none of the peaks are completely suppressed, showing that they are not ghost peaks. For **Cu6**, the longer distance peak (around 3.8 nm) shows the largest difference, but this distance was already considered non reliable after validation. For **Cu8**, small differences are also observed for the small feature between 3.5 and 4 nm. In the latter case, it appears that the peak shifts to a different distance, suggesting even more care when interpreting this distance.

Expected distances for the Cu cages

From quantum-mechanical calculations, model structures for **Cu6** and **Cu8** were obtained [7]. For **Cu6** and **Cu8**, two possible structures were found, which differ in the location of the Cu ions and thereby the Cu-Cu distances. In figure SI1, both models are shown. As described in detail in Bobylev *et al.* [7], for **Cu6** model 1, the Cu ions are located in the six square windows of the nanosphere, creating a shape close to an octahedron, see figure 1A, whereas in model 2, four copper ions are located below a palladium center and two in the square windows of the nanosphere (see SI for comparison of models 1 and 2 for **Cu6** and **Cu8** respectively). For **Cu8,** model 1, with the Cu-ions in the triangular windows, the copper ions are located at the corners of a cube, see figure 1B and SI1, while in model 2, six copper-ions are in the square windows and two in the triangular windows, forming a distorted cube (see figure SI1). For **Cu6** and **Cu8**, the models predict different Cu-Cu distances, see table 1, suggesting that the DEER distances could help in deciding between models.

For **Cu6**, the distances found by DEER agree slightly better with model 1, in agreement with conclusions drawn from other experimental evidence in Bobylev *et al.* [7]. For **Cu8**, the distances that are predicted for the two models overlap within their uncertainty margins, largely because in model 2 the deviation from a ideal cube is quite large. The DEER distances fall within the range of both models. Model 1 predicts two distances (2.0 and 2.8 nm) that are close to the experimental ones and a long distance (3.4 nm) that is not observed. The latter distance may be difficult to observe in the DEER experiments, see discussion. In

contrast to the situation in **Cu6**, the experimental distances do not enable to distinguish between the models, see discussion.

In principle, each pair of Cu ions within the distance range of the DEER experiment is expected to contribute to the distance distributions. Considering the geometric structure of the cages according to model 1 (figure 1), each Cu(II) ion has multiple neighbors with a distance within the DEER range. The expected intensity ratios of the distance peaks are given in table 1. For **Cu6**, model 1, each Cu(II) ion has four neighbors at a distance of 1.9 nm, and one at a distance of 2.7 nm, so the expected intensity ratio of the two distance peaks would be 4:1. For **Cu8,** model 1, each Cu(II) ion is expected to have three neighbors at 2 nm, three at 2.8 nm and one at 3.4 nm, so the expected ratio of the distance peaks is 3:3:1. The same holds for model 2, as long as it can be considered an almost ideal geometrical body.

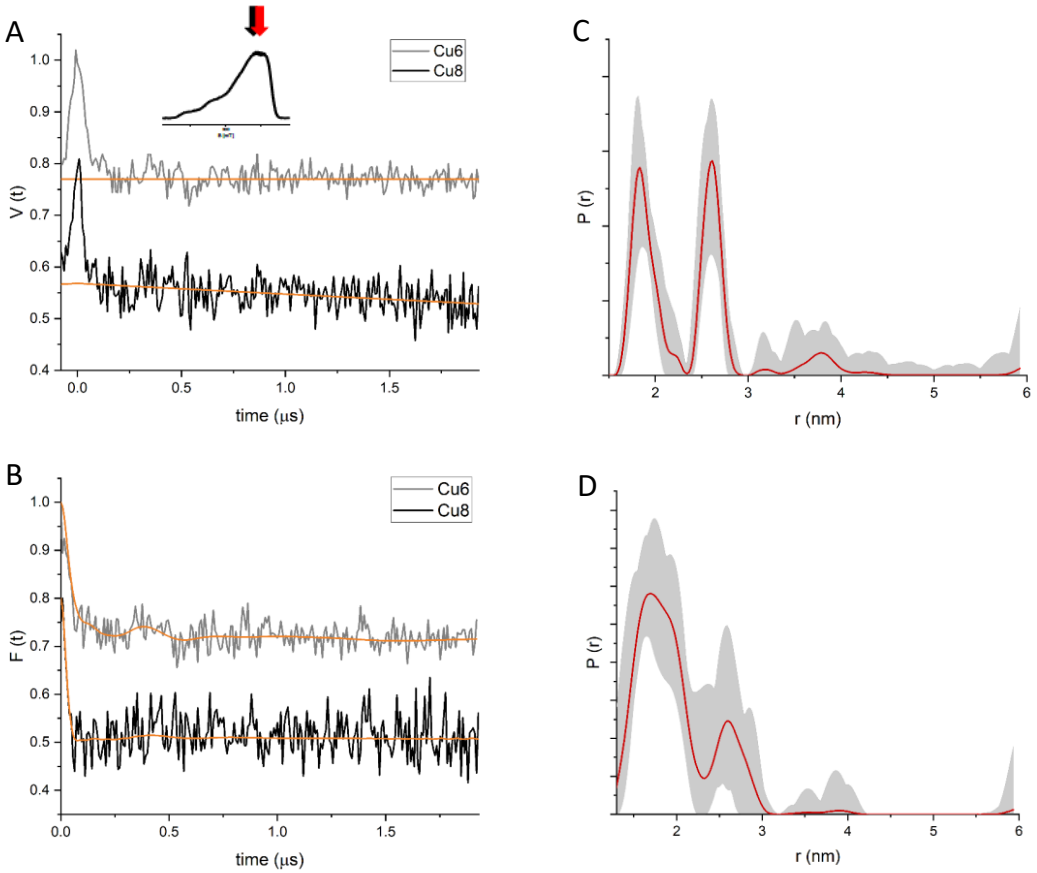

Figure 2. Results of DEER experiments of the **Cu6** and **Cu8** cages. A) Raw DEER traces. Gray: **Cu6**, black: **Cu8**. Orange: background. B) Background subtracted DEER traces with fits (orange). Gray: **Cu6** trace, black: **Cu8**. C) Distance distribution obtained for **Cu6** (red). D) Distance distribution obtained for **Cu8** (red). Maximum echo intensity (A,B) is normalized to unity, **Cu8** traces have been downshifted for better visibility. Shaded area in C) and D): standard deviation of each point in the distance distribution, by validation DEERAnalysis. Inset: field-swept-echo EPR spectrum of **Cu6**. Arrows: position of pump (red) and observer (black) frequency. V(t) : primary measured data, normalized to maximum intensity. F(t) : form factor obtained after background subtraction. For details and experimental parameters, see text.

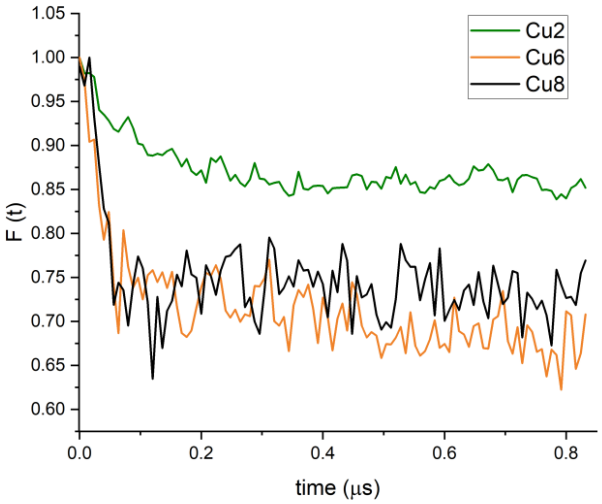

Figure 3**.** Comparison of the modulation depth of **Cu6** and **Cu8** with that of **Cu2**. DEER traces (background subtracted) obtained for **Cu6**, **Cu8** and **Cu2,** containing two Cu(II) ions at a distance of 3.3 nm. Green trace: **Cu2**, orange: **Cu6,** black: **Cu8**. Modulation depth of **Cu2** λ = 13%. In all traces maximum DEER-trace intensity is normalized to unity. For better S/N ratio, traces of **Cu6** and **Cu8** have shorter evolution time than in Fig. 2.

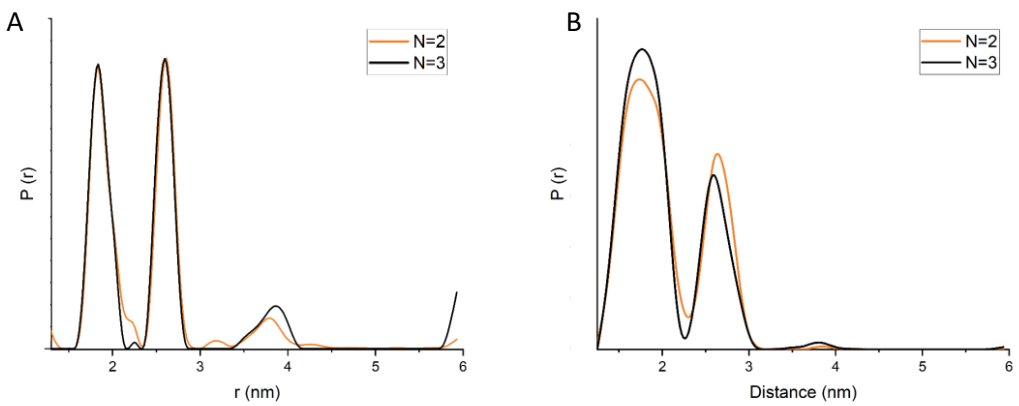

Figure 4. Effect of ghost suppression on distance distribution for three (N = 3) spins, compared with distance distribution for two (N = 2) spins. A) Effect of ghost suppression on **Cu6**. B) **Cu8**. Orange: distance distribution obtained without ghost suppression N = 2, black: distance distribution obtained with ghost suppression for N=3 spins. The areas below the P(r) curves were normalized to unity.

Table 1. DEER distances, modulation depth and model-derived distances for **Cu6** and **Cu8**. <r>: center of peak. Δ: measured modulation depth of the background-subtracted DEER traces. The expected intensity ratio is valid for both model 1 (M1) and model 2 (M2). DEER results are processed by Tikhonov regularization. Uncertainty for distances in model are derived from variations in Cu-Cu distances of

Cu6 distances from DEER	**Cu6 M1**	**Cu6 M2**	**expected intensity ratio Cu6**	**Cu6 Δ %**	**Cu8 distances from DEER**	**Cu8 M1**	**Cu8 M2**	**expected intensity ratio Cu8**	**Cu8 Δ %**
<r> (nm)	**r (nm)**	**r (nm)**		**23 ± 2**	**<r> (nm)**	**r (nm)**	**r (nm)**		**22 ± 2**
1.8	**1.8 ± 0.3**	**1.7 ± 0.3**	**4**		**1.8**	**2.0 ± 0.1**	**2.2 ± 0.6**	**3**	
2.6	**2.6 ± 0.3**	**2.7 ± 0.2**	**1**		**2.6**	**2.8 ± 0.1**	**3.1 ± 0.6**	**3**	
						3.5 ± 0.14	**3.8 ± 0.2**	**1**	

5.4 Discussion

Distance determination in multi-spin systems is an important extension to standard pair-distance determination by DEER. Up to now, such interactions were mostly investigated for nitroxide, trityl and Gd(III) systems [28, 30, 35-38]. The Cu(II)-cages, **Cu6** and **Cu8**, investigated here, represent an interesting model case that enables to extend multi-spin interactions to systems with a larger anisotropy. Two Cu-cages were investigated, comprising six (**Cu6**) and eight (**Cu8**) Cu(II) ions, respectively, in cage-like arrangements (see

figure 1). The structure of the cages was determined by a variety of techniques, as described in [7], where also their synthesis and properties are described. Here we describe the detailed investigation of these copper cages by DEER spectroscopy, to determine the distances between the Cu(II) ions and the impact of multispin interaction.

For both **Cu6** and **Cu8,** two models were proposed that differ in the location of the copper ions within the cage. For **Cu6** the measured distances are in slightly better agreement with those predicted from model 1, see table 1. That assignment agrees with other experimental results and firmly places the copper ions in the square windows of the Pd-ions, as shown in figure 1B. Whereas the distances observed in the DEER experiment agree well with those expected (table 1), the intensity of the DEER distance peaks deviate: The relative intensities of the distance peaks is 1:1, while 4:1 is expected (see table 1). Possible reasons for the too low intensity of the shorter distance peak (1.8 nm), amongst which orientation selection, are discussed in the SI. For **Cu8**, the predicted structure for model 2 deviates strongly from a cube, leading to larger deviations between Cu-Cu distances that would be identical in the cube. As a result, the model distances do not allow to discriminate between model 1 and model 2 for **Cu8**. Also, the overall lower signal-to-noise ratio of the **Cu8**-DEER traces, compared to **Cu6**, contributes to the difficulty. One causal factor is the shorter T_2 relaxation time of **Cu8** compared to **Cu6** (see SI). Comparison to model 1 (table 1) shows that the two shorter distances are not too far from the expectation from model 1, a third, longer distance, is missing (table 1). Even though the distance at 3.4 nm represents a single Cu-Cu pair and therefore could have a lower contribution to the distance distribution, at the expected ratio of 3:3:1 (table 1) it should still be seen. An explanation for the absence of the long distance peak for **Cu8** (3.4 nm in model 1) could be the uncertainty in the background correction in combination with the relatively short evolution time. In view of the deviations of model, is model 2 perhaps a better model? As model 2 does not account for the dominant distance of 1.7 nm measured (table 1), this does not seem to be the case. This leads to a preference for model 1, however with much less confidence than for **Cu6**, especially since also other experimental results [7] could not discriminate between the two models for **Cu8**. Possible scenarios for **Cu8** could be that the copper ligands, e.g. the pyrrolidine ligands [7], have different orientations, leading to a spread in copper positions and thereby broader distance distributions, or a coexistence of the two **Cu8** model structures, which would result in a superposition of the respective distances. Both possibilities could also lead to the larger width and more asymmetric shape of the distance peaks in **Cu8** compared to **Cu6**. Summarizing, all peaks observed in the distance distributions in **Cu6** and **Cu8** are accounted for by the expected pairwise distances. The distances found for **Cu6** and **Cu8** are reliable, since ghost suppression does not abolish any of the distance peaks, revealing that all

distance peaks of **Cu6** and **Cu8** are real. Additionally, as all peaks observed correspond to distances expected for the Cu-cages, full suppression of individual peaks is not likely.
The larger modulation depth of **Cu6** and **Cu8** compared to the reference compound (see results, Fig. 4) clearly shows that more than two spins interact, however, the number of interacting spins is lower than six (**Cu6**) resp. eight (**Cu8**), and several sources can contribute to the lower number. The uncertainty in the number of interacting spins derives from the signal-to-noise ratio of the DEER data (fig. 3) of both, the Cu-cages, and the reference compound (**Cu2**). Other effects, such as orientation selection and chemical factors, for example reduction of some of the Cu(II) centers in the cages, are difficult to quantify, but they would all lower the number of interacting spins, as described in the SI. Experimentally, some of these factors could be tackled, however, given the fragility of these samples this was not feasible (for details, see SI). Also, short phase memory time, T_m causes problems. Consequently, both Cu-cages display multispin properties, yet, the factors described result in a number of interacting spins that is significantly lower than expected, considering that there are six, respectively eight Cu centers in the two cages.
Both, theoretical studies of multispin effects [26-28] and experimental results [23, 36, 39] described in the literature, showed rather strong multispin effects on DEER distance distributions. In view of these results, the effects shown in figure 4 and figure SI5 and SI6 are weak. An obvious difference is that most of the systems described in the literature so far are nitroxide based. Nitroxides have a smaller spectral anisotropy than the Cu(II) centers investigated here, resulting in a higher pump-pulse-inversion efficiency λ for nitroxides compared to Cu(II). A clear indication of the small λ of the Cu(II) systems investigated here is the modulation depth Δ of only 13 % for **Cu2**, a two-Cu(II) system with λ = Δ, whereas for two-spin interactions in nitroxides modulation depths of around 50 % are standard at 9.5 GHz DEER [18]. Low pump-pulse-inversion efficiency also translates to low multispin excitation and thereby low ghost-peak intensities, as Edwards et al. have shown [30]. In the latter work, nitroxides had stronger ghost-peak contributions than Gd(III) labels, in agreement with the larger spectral anisotropy of Gd(III) with respect to nitroxides [30]. Evidently, this is also the case for the copper cages. Additionally, it was shown that multispin effects can be suppressed by lowering the inversion efficiency and power scaling [26-28].
The relative intensities of the distance peaks differ from those expected from the model, see above. One explanation could be that the intensitites are affected by ghost-peak effects. For example, Valera *et al.* [28] found that not in all cases ghost-peak suppression recovers the expected distance-peak intensities. Also, orientation selection could play a role, see SI, however, no quantitative estimate can be given at this point.
In conclusion, the two copper cages **Cu6** and **Cu8**, show that multispin effects can also be tackled in Cu(II)-based systems and that DEER is an excellent tool to obtain structure

information in multi-copper systems. This extends the reach of DEER for multispin systems, whether biological or chemical, be it for catalysis systems or those of interest for material sciences.

Supplementary Information

Meaning of geometric interpretation, Cu8: cube, Cu6: octahedron

The description of the arrangement of the Cu-ions in the cages as a cube (**Cu8**) or an octahedron (**Cu6**) facilitates the description of the arrangement of the Cu-ions, but does not imply that the ions form an idealized geometric body. The uncertainty range for the distances obtained from the models (Table 1, main text) gives the range of distances of individual pairs of Cu-ions. In an ideal cube or octahedron all distances between the specific types of Cu-ions should be identical. However, especially the model 2 structures show clear deviations from the shapes, as seen in figure SI1, where the distortions already can be seen in the figure.

The corners of polyhedra also have specific relations between distances: In a cube, the relation between the shortest distance (distance ***a***) along the edge of the cube and the face-diagonal (distance ***b***) is $\boldsymbol{b} = 1/\sqrt{2}\,\boldsymbol{a}$, the same as the ratio between the shorter and the longer distance in an octahedron. As a result, the distances in **Cu6** and **Cu8** are expected to follow this ratio.

Overview of measurement

The DEER traces presented here can be compared to those shown in Bobylev *et al.* [7]. For **Cu6**, increasing the accumulation time and optimizing the pulse-excitation resulted in a better signal-to-noise ratio, increasing the confidence level for the distance-distribution shape compared to the traces shown in figure 8 and 10 of [7], while leading to the same distances as before. For **Cu8**, several attempts to improve the signal-to-noise ratio in a similar way did not improve the data due to a combination of factors, suggesting that the shorter T_m time or other chemical factors cause the lower signal-to-noise ratio compared to what can be achieved for **Cu6**. In [7] DEER was one of several methods to verify the structure of the cages, so the focus was on the distances only. In the present manuscript, the number of interacting spins is determined by a direct comparison with a two-copper model compound (**Cu2**) enabling detailed analysis of this point in the multi-copper systems investigated. Additionally several different analysis methods were applied (Gaussian analysis of DEER traces, and DeerNet), see below, to quantitate the reliability of the analysis. Most of the differences observed with respect to [7], such as that the second distance peak in the **Cu8** distance distribution centered at 2.6 nm, see figure 2, is reliable, result in a higher confidence in the interpretation and are due to the better signal to noise ratio of the data.

Reproducibility was checked by measuring samples multiple times, and also measuring samples that had not been measured before. In between measurements, the EPR tubes with

the samples were stored in liquid nitrogen, and introduced into the precooled resonator, to avoid accidental warming of the samples as much as possible.

Possible orientation selection effects in the DEER traces

As mentioned in the main text, orientation-selection effects can lead to a reduction of the copper-copper interaction observed by DEER, which reduces the modulation depth, i.e. the total number of spins interacting (see discussion main text). Also, orientation selection can affect specific pairs of spins more strongly than others, which would cause a deviation of the relative intensity of the distance peaks from the expected intensities given in table 1, main text. In the DEER experiments, both the pump- and the observer frequencies were positioned in the perpendicular region of the EPR spectrum, see figure 2 main text and figure SI3. Therefore, spin pairs in which the parallel component, i.e. g_{zz}, of the g-tensor of one Cu(II) is parallel to the perpendicular component, i.e. the g_{xx}-g_{yy} plane, of the other Cu(II) will not contribute to the DEER effect, because for these pairs only one of the two partners are excited. The actual orientation of g-tensors of pair could also be in between the extremes, leading to partial excitation of a pair, for example. Consequently, the relative orientation of the g-tensors of two coppers in the cages determines how much these two Cu(II) centers contribute to the DEER effect. This can lead to reduced or absent DEER effects for specific pairs. As the g-tensor directions of the Cu(II)-centers in the Cu-cages are not known, the contribution of this effect cannot be estimated. Experimentally, orientation effects can be determined by setting the pump-pulse to a parallel and the observer pulse to a perpendicular position in the EPR spectrum, and vice versa, however, for Cu(II), the limited bandwidth of the resonator does not allow this. Other approaches have been used as well, see [40-43], however, in the present case, the sensitivity was not sufficient to measure meaningful DEER traces in the parallel region of the spectrum, as would be needed to use such an approach. Thus, orientation-selection effects can effectively lower the number of spins observed, and can lead to a difference in the relative intensity of distance peaks from those expected, see below.

Applying different analysis methods for DEER data

Different analysis methods for the DEER data were tested to (i) determine the reliability of the analysis described in the main text and (ii) to investigate if other interpretations are compatible with the data.

(i) The DeerNet analysis (figure SI 9 and 10) shows that also the shape of the distance distribution is robust and agrees with the Tikhonov analysis, as confidence levels and shape agree. For using DeerNet, unfortunately, the signal-to-noise ratio (12 for **Cu6** and 9 for **Cu8**) is at or below the limit of the S/N-ratio recommended in DeerNet. So in this case, the

advantage of the DeerNet program, namely that processing of baseline and form factor is user-invention free [44, 45], cannot be fully harnessed: The simulated form-factor contribution, especially for **Cu8**, figure SI 10A, is less smooth than we would chose. The DEERNet option to do Tikhonov analysis shown in Fig. SI 9B and 10B can be directly compared to that in Fig. 2B, main text, showing that a smaller regularization parameter selected in the user-adjusted Tikhonov regularization smoothens out some of the features that we interpret as noise. So we see that in this very specific case, while DeerNet confirms the overall distance distribution, and unambigously quantifies trace parameters such as the signal-to-noise ratio, it cannot be used as the only method of data analysis.
(ii) Analysis of the data with Gaussian distance distributions enables to change distance parameters, such as center-distance and -width of the distance peaks individually. Here we checked if the distance peaks could have different widths, however, as figure SI7 and SI8 show, the optimum solution is similar to the Tikhonov one.
Also, we tested if different relative weights of the distance peaks were compatible with the data, given that the expected intensity of the distance peaks (see Tab. 1, main text) deviates from those found in Tikhonov analysis.
We found that for **Cu6**, changing the weight by more than 25 %, maintaining the width constant, results in significant deviation from the experimental DEER curve (data not shown), revealing that the deviation of the relative weights of the respective distances from the expected intensity ratios of the distance peaks (table 1, main text) is outside the experimental uncertainty. In the case of **Cu8**, also simulating with two Gaussian distance peaks is possible, (data not shown), probably attributable to the intrinsically low population of the third distance peak at 3.4 nm. For these tests, the distance and the width of the distance peaks were kept within a narrow range, so it cannot be excluded that larger variations of the relative weights of the distance peaks would be possible if the other parameters are changed more extensively. Due to the overall low signal-to-noise ratio of the data we did not expect unambiguous solutions.

Modulation depth and the relative intensities of the distance peaks

Deviations of the intensity of the distance peaks (figure 2, main text) from the expected intensities (Table 1 main text) can be due to incomplete ghost-peak supression in multispin systems as described in the main text. Specific factors can also enter: For **Cu6**, instead of the expected ratios of 4:1 (1.8 nm relative to 2.6 nm peak, figure 2) the distance peak at 1.8 nm is somehwat broadened, but not four times more intense than the distance peak at 2.6 nm. One reason could be a less favorable orientation selection for the Cu-pairs at the shorter distance, resulting in a smaller probability to excite just these pairs, and thereby causing lower intensity of the specific distance peak, see above. Also, the model predicts that the

distance between some Cu-pairs may be as short as 1.5 nm. For such short distances, the excitation bandwidth of the pulses would not be sufficient, resulting in a smaller contribution of these distances, and thereby, again, a smaller intensity for the distance peak at 1.8 nm. We tested this with the limited-bandwidth-excitation feature in DeerAnalysis but found only small changes, so it is probably not the main factor contributing. For **Cu8**, similar arguments than for **Cu6** can be made. In addition, the overall broader lines in the distance distribution could be an indication that, as seen in model 2, multiple conformations contribute and that the superposition of those conformations of the cage smear out the distance peaks.

Why not all spins in the cages are observed

Several factors contribute to the uncertainty of the number of interacting spins determined: Measurement and interpretation of the modulation depth requires that sample and reference are measured with precisely the same conditions. Therefore, measurements were performed in the same experimental run, to minimize day to day variations, and with shorter evolution times to improve signal-to-noise ratios. Also, the spectra of sample and reference must have similar anisotropies. As figure SI3 shows, the EPR spectra of the Cu-cages and the reference compound almost overlap, showing that this condition is fulfilled. Several other factors, such as orientation selection (see above) and partial reduction the Cu-ions in the cages [7] , can lead to a smaller number of spins measured than expected. Another factor that can reduce modulation depth is a contribution of short distances, since for short distances, the excitation bandwidth of the pulses is not sufficient to excite the dipolar interaction. As a result, pairs at very short distances, roughly below 1.6 nm at our experimental conditions, would contribute less, or not at all to the modulation depth. This may contribute here, as the DEER time traces (figure 2, main text) show a fast initial decay, suggesting a contribution of spin-pairs at short distances, and, for **Cu6**, the models show distances can be as short as 1.5 nm. Also, orientation selection, described above, can cause specific pairs of spins to contribute less to the modulation depth than others. As several of the factors described reduce the modulation depth, the measured value can be considered as a lower limit.

Supplementary figures

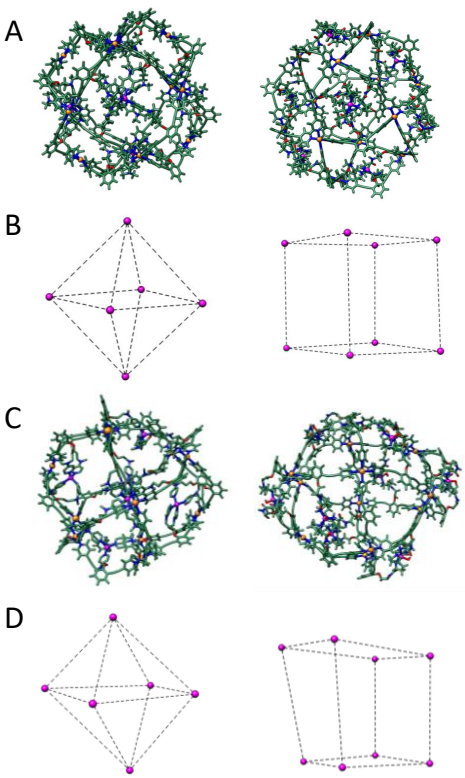

Figure SI.1. Model structures of copper cages. A) Model 1 structures. B) Relative position of the copper ions in model 1. C) Model 2 structures. D) relative position of the copper ions in model 2. Left: **Cu6**, right: **Cu8**. Orange: Palladium, Magenta: Copper ions. See main text and Bobylev *et al.* [7].

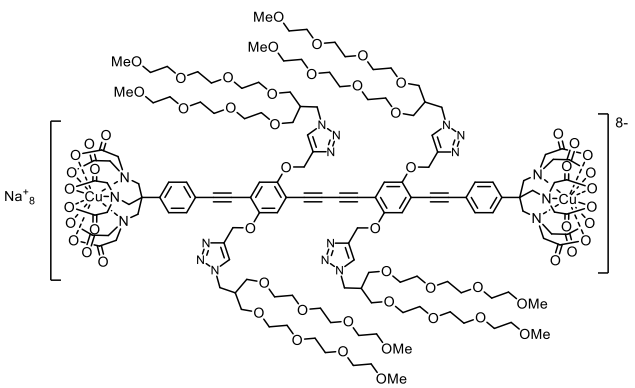

Figure SI.2. Structure of **Cu2**, used as a two copper reference. For details, see main text.

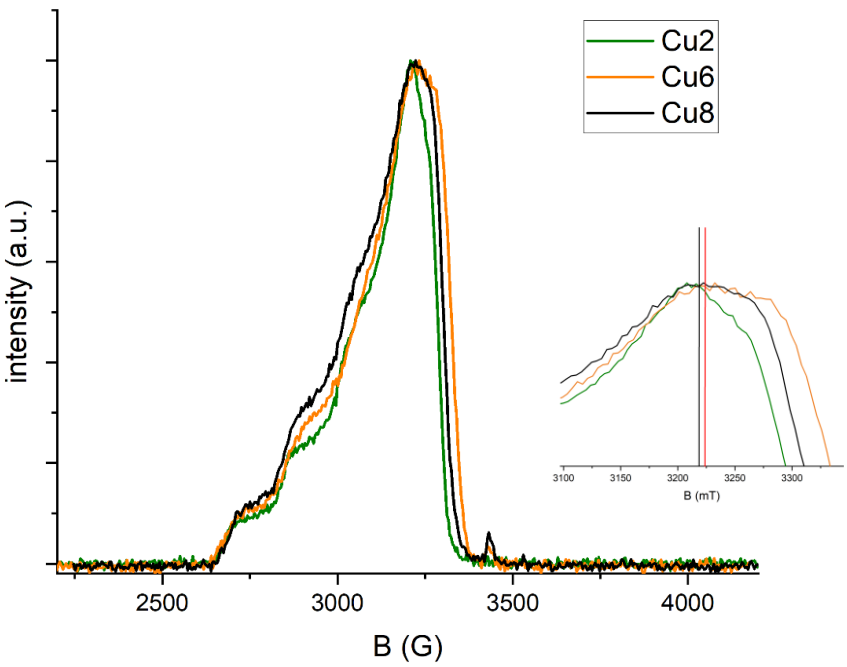

Figure SI.3. Field swept echo detected EPR spectra of all compounds. Green: **Cu2**, orange: **Cu6**, black: **Cu8**. Spectra were baseline corrected and normalized to maximum intensity. Overall similarity of spectra suggests that excitation in DEER is similar, but differences in orientation selection cannot be excluded (see text). The lines in the inset indicate position of the pump (red) and observer (black) pulses.

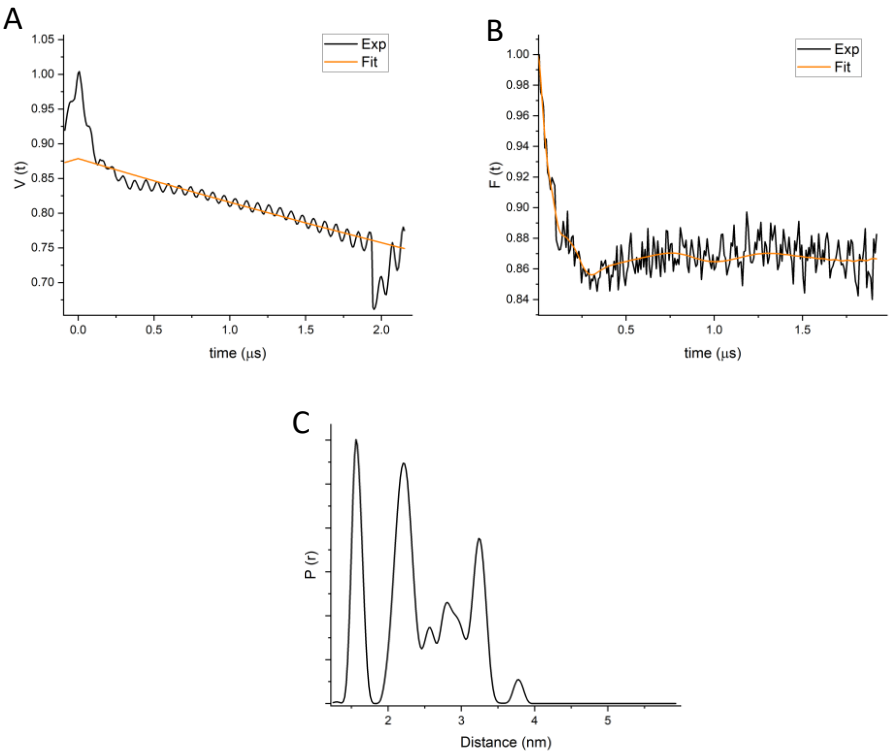

Figure SI.4. Results of DEER experiments with **Cu2**. A) Raw DEER trace (black) background (orange). B) Background subtracted DEER trace (black) with fit (orange). Maximum echo intensity (A,B) is normalized to unity. V(t) : primary measured data, normalized to maximum intensity. F(t) : form factor obtained after background subtraction. For details and experimental parameters, see text. C) Distance distribution obtained for **Cu2:** expected distance is 3.3 nm. It was shown in Keller *et al.* [9] that several peaks of the distance distribution derive from contributions of weak exchange-coupling, for which we do not correct here. Peak at 1.5 nm: possible artifact for non-completely suppressed proton modulation.

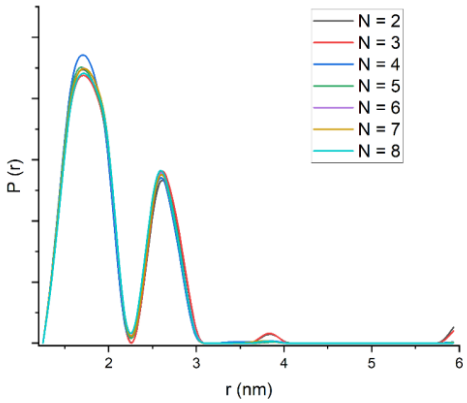

Figure SI.5. Effect of ghost suppression on **Cu8** distance distribution, from N = 2 to to N = 8, eight interacting Cu(II). For details, see Materials and Methods section and main text.

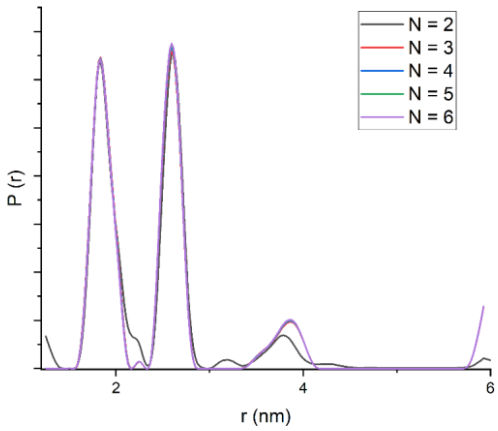

Figure SI.6. Effect of ghost suppression on **Cu6** distance distribution, from N = 2 to N = 6. For details, see Materials and Methods section and main text.

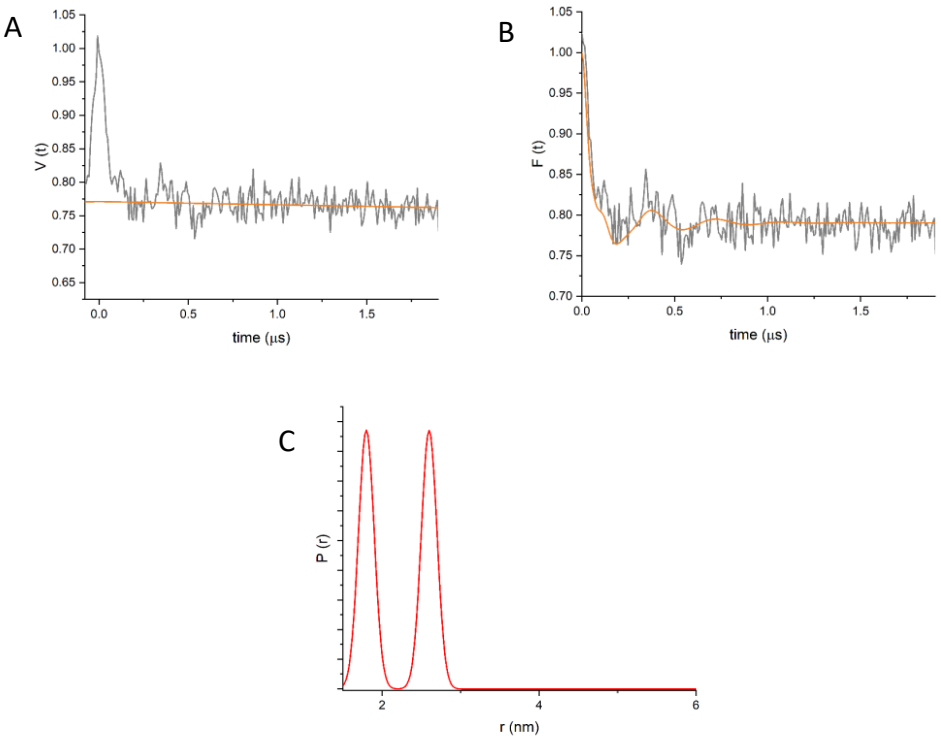

Figure SI.7. **Cu6** data analyzed with two-Gaussian fitting in DeerAnalysis. A) DEER trace (grey) and background (orange), B) background subtracted trace (grey) and fit (orange) C) distance distribution. N=2 spins, and two Gaussian peaks centered at 1.8 and 2.6 nm. Manually changing the width or center of the Gaussians did not significally improve the agreement with the data. For details, see text.

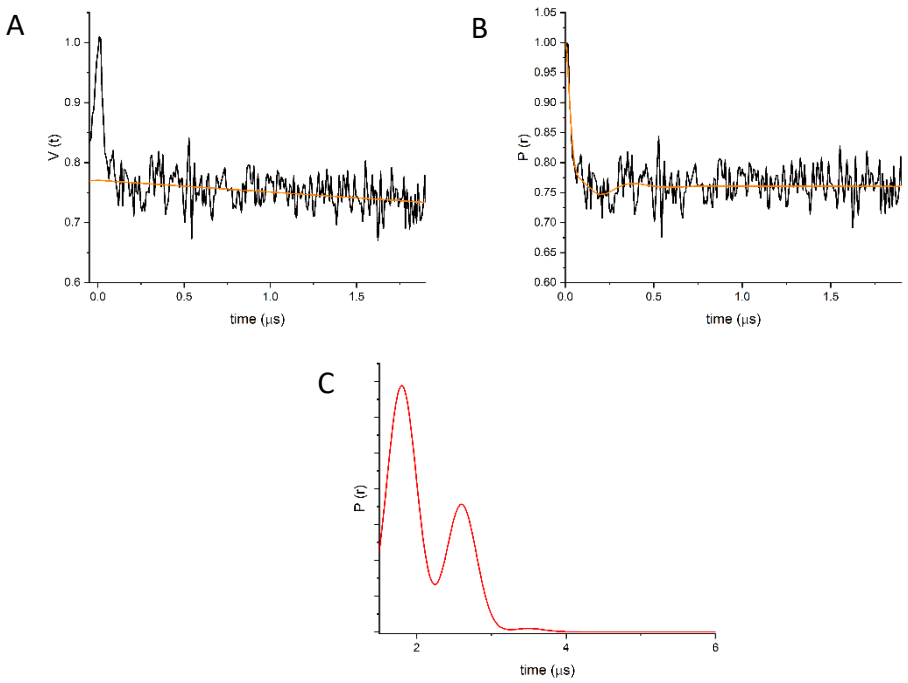

Figure SI.8. **Cu8** data analyzed with three-Gaussian fitting in DeerAnalysis. A) DEER trace (black) and background (orange), B) background subtracted trace (black) and fit (orange) C) distance distribution. N=2 spins, and three Gaussian peaks centered at 1.8, 2.6 and 3.5 nm. Manually changing the width or center of the Gaussians did not significally improve the agreement with the data. For details, see text.

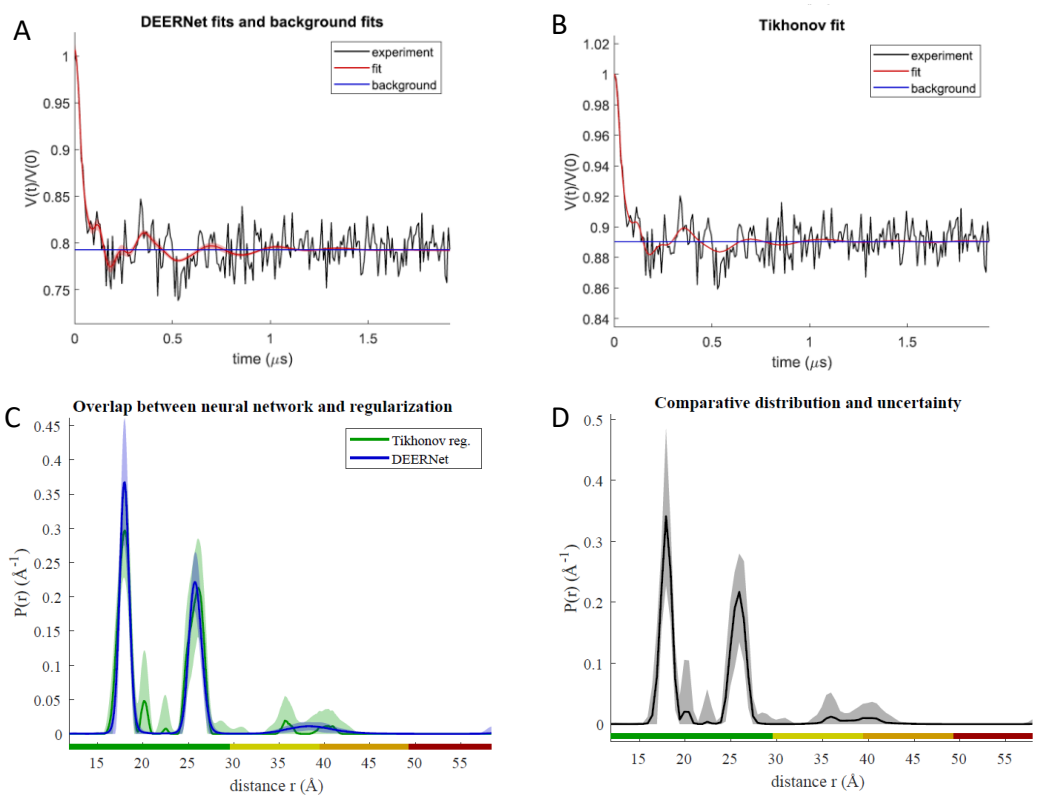

Figure SI.9. **Cu6** data analyzed with DEERNet tool in DeerAnalysis 2023. A) Deer trace (black), background (blue), fit (red) from DEERNet. B) Deer trace (black), background (blue), fit (red) from Tikhonov regularization. C) distance distribution, comparison between DEERNet (blue) and Tikhonov regularization (green). D) Comparative distribution from C). Shaded area in C) and D): uncertainty margins. The colors on the abscissa axis of the distance distribution indicate reliability of distance peaks: green: shape of distance distribution is reliable, yellow: mean distance and width are reliable, orange: mean distance is reliable, red: distance may be detectable, but cannot be quantified. Compared to the Tikhonov results shown in the main text (Figure 2), the regularization parameters is larger, which we consider an over-interpretation of the data.

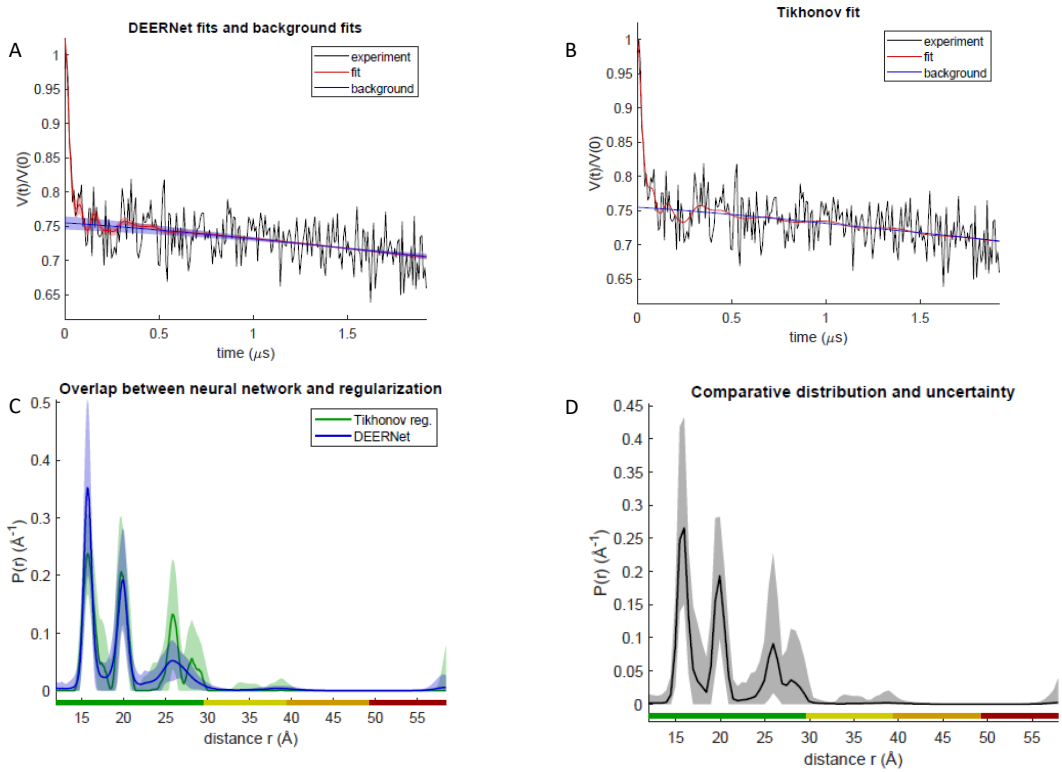

Figure SI.10. **Cu8** data analyzed with DEERNet tool in DeerAnalysis 2023. A) Deer trace (black), background (blue), fit (red) from DEERNet. B) Deer trace (black), background (blue), fit (red) from Tikhonov regularization. C) distance distribution, comparison between DEERNet (blue) and Tikhonov regularization (green). D) Comparative distribution from C). Shaded area in C) and D): uncertainty margins. The colors on the abscissa axis of the distance distribution indicate reliability of distance peaks: green: shape of distance distribution is reliable, yellow: mean distance and width are reliable, orange: mean distance is reliable, red: distance may be detectable, but cannot be quantified. Overall, DEERNET confirms results presented in main text. In contrast to the Tikhonov results shown in figure 2 (main text), the main peak at 1.7 nm is split into two peaks (1.6 and 2.0 nm), however, the data are at the lower end of the recommened signal to noise ratio for DeerNet. Compared to the Tikhonov results shown in the main text, the regularization parameters is larger, which we consider an over-interpretation of the data. Overall, DEERNet confirms results presented in main text.

Table SI 1 Measured relaxation time constants for the cages **Cu6** and **Cu8**. T_m: phase-memory time. T_1: spin-lattice-relaxation time. The T_m relaxation was measured with the two-pulse sequence (π/2)-τ- (π)- τ-[echo] with an initial τ of 200 ns and 4 ns step increments. The T_1 relaxation was measured with the inversion-recovery sequence (π)- T-(π/2)-τ- (π)- τ-[echo]. The τ value was kept constant at 200 ns, starting T value was 400 ns with 40 ns step increments. 16 ns length for π/2 pulses and 32ns for π pulses were used. The T_m and T_1 time constants were obtained through exponential fitting. Measurement temperature: 30K.

	Cu6	**Cu8**
T_m (ns)	**522 ± 11**	**302 ± 7**
T_1 (µs)	**8.7 ± 0.4**	**15.4 ± 0.5**

References

[1] M.J. Wiester, P.A. Ulmann, C.A. Mirkin, Enzyme mimics based upon supramolecular coordination chemistry, Angew Chem Int Ed Engl 50(1) (2011) 114-37.
[2] T. Brugnari, D.M. Braga, C.S.A. dos Santos, B.H.C. Torres, T.A. Modkovski, C.W.I. Haminiuk, G.M. Maciel, Laccases as green and versatile biocatalysts: from lab to enzyme market—an overview, Bioresources and Bioprocessing 8(1) (2021).
[3] R. Guo, J. Gu, S. Zong, M. Wu, M. Yang, Structure and mechanism of mitochondrial electron transport chain, Biomed J 41(1) (2018) 9-20.
[4] P. Brzezinski, A. Moe, P. Adelroth, Structure and Mechanism of Respiratory III-IV Supercomplexes in Bioenergetic Membranes, Chem Rev 121(15) (2021) 9644-9673.
[5] M. Ruben, J.M. Lehn, P. Muller, Addressing metal centres in supramolecular assemblies, Chem Soc Rev 35(11) (2006) 1056-67.
[6] L. Chen, Z. Guo, X.G. Wei, C. Gallenkamp, J. Bonin, E. Anxolabehere-Mallart, K.C. Lau, T.C. Lau, M. Robert, Molecular Catalysis of the Electrochemical and Photochemical Reduction of CO2 with Earth-Abundant Metal Complexes. Selective Production of CO vs HCOOH by Switching of the Metal Center, J Am Chem Soc 137(34) (2015) 10918-21.
[7] E.O. Bobylev, L. Passerini, F.J. de Zwart, D.A. Poole, S. Mathew, M. Huber, B. de Bruin, J.N.H. Reek, Pd12MnL24 (for n = 6, 8, 12) nanospheres by post-assembly modification of Pd12L24 spheres, Chemical Science 14 (2023) 11840-11849.
[8] B. Huang, L. Mao, X. Shi, H.B. Yang, Recent advances and perspectives on supramolecular radical cages, Chem Sci 12(41) (2021) 13648-13663.
[9] K. Keller, I. Ritsch, H. Hintz, M. Hülsmann, M. Qi, F.D. Breitgoff, D. Klose, Y. Polyhach, M. Yulikov, A. Godt, G. Jeschke, Accessing distributions of exchange and dipolar couplings in stiff molecular rulers with Cu(II) centres, Phys Chem Chem Phys 22(38) (2020) 21707-21730.
[10] Y. Ozaki, M. Kawano, M. Fujita, Engineering noncovalent spin-spin interactions in an organic-pillared spin cage, Chem Commun (Camb) (28) (2009) 4245-7.
[11] K. Nakabayashi, Y. Ozaki, M. Kawano, M. Fujita, A self-assembled spin cage, Angew Chem Int Ed Engl 47(11) (2008) 2046-8.
[12] W.L. Jiang, Z. Peng, B. Huang, X.L. Zhao, D. Sun, X. Shi, H.B. Yang, TEMPO Radical-Functionalized Supramolecular Coordination Complexes with Controllable Spin-Spin Interactions, J Am Chem Soc 143(1) (2021) 433-441.
[13] S.A.D. K. M. SALIKHOV, AND A. M. RAITSIMRING, The Theory of Electron Spin-Echo Signal Decay Resulting from Dipole-Dipole Interactions between Paramagnetic Centers in Solids, jOURNAL OF MAGNETIC RESONANCE 42 (1981) 255 - 276.
[14] M. Pannier, S. Veit, A. Godt, G. Jeschke, H.W. Spiess, Dead-time free measurement of dipole-dipole interactions between electron spins. 2000, J Magn Reson 213(2) (2011) 316-25.
[15] F.D. Breitgoff, K. Keller, M. Qi, D. Klose, M. Yulikov, A. Godt, G. Jeschke, UWB DEER and RIDME distance measurements in Cu(II)-Cu(II) spin pairs, J Magn Reson 308 (2019) 106560.
[16] M.U. Irene M. C. van Amsterdam, Gerard W. Canters, and Martina Huber, Measurement of a Cu-Cu Distance of 26 A by a Pulsed EPR Method, Angew. Chem. Int. Ed 42(1) (2003) 62-64.

[17] M.M. Roessler, M.S. King, A.J. Robinson, F.A. Armstrong, J. Harmer, J. Hirst, Direct assignment of EPR spectra to structurally defined iron-sulfur clusters in complex I by double electron-electron resonance, Proc Natl Acad Sci U S A 107(5) (2010) 1930-5.
[18] G. Jeschke, DEER distance measurements on proteins, Annu Rev Phys Chem 63 (2012) 419-46.
[19] O. Schiemann, C.A. Heubach, D. Abdullin, K. Ackermann, M. Azarkh, E.G. Bagryanskaya, M. Drescher, B. Endeward, J.H. Freed, L. Galazzo, D. Goldfarb, T. Hett, L. Esteban Hofer, L. Fabregas Ibanez, E.J. Hustedt, S. Kucher, I. Kuprov, J.E. Lovett, A. Meyer, S. Ruthstein, S. Saxena, S. Stoll, C.R. Timmel, M. Di Valentin, H.S. McHaourab, T.F. Prisner, B.E. Bode, E. Bordignon, M. Bennati, G. Jeschke, Benchmark Test and Guidelines for DEER/PELDOR Experiments on Nitroxide-Labeled Biomolecules, J Am Chem Soc 143(43) (2021) 17875-17890.
[20] D.M. Bela E. Bode , Jorn Plackmeyer , Gerd Durner, Thomas F. Prisner, Olav Schiemann, Counting the monomers in nanometer-sized oligomers by pulsed electron-electron double resonance, JACS 129 (2007) 6736-6745.
[21] A.D.Milov, Yu.D.Tsvetkov, F.Formaggio, M.Crisma, C.Toniolo, a. J.Raap, The Secondary Structure of a Membrane-Modifying Peptide in a Supramolecular Assembly Studied by PELDOR and CW-ESR Spectroscopies, J. Am. Chem. Soc. 123 (2000) 3784-3789.
[22] A. D. Milov, Yu. D. Tsvetkov, a.J. Raap, Aggregation of Trichogin Analogs in Weakly Polar Solvents: PELDOR and ESR Studies, Appi. Magn. Reson 19 (1998) 215-226.
[23] M.J. Junk, H.W. Spiess, D. Hinderberger, DEER in biological multispin-systems: a case study on the fatty acid binding to human serum albumin, J Magn Reson 210(2) (2011) 210-7.
[24] E.R. Georgieva, P.P. Borbat, H.D. Norman, J.H. Freed, Mechanism of influenza A M2 transmembrane domain assembly in lipid membranes, Sci Rep 5 (2015) 11757.
[25] P.S. Kerry, H.L. Turkington, K. Ackermann, S.A. Jameison, B.E. Bode, Analysis of influenza A virus NS1 dimer interfaces in solution by pulse EPR distance measurements, J Phys Chem B 118(37) (2014) 10882-8.
[26] T. von Hagens, Y. Polyhach, M. Sajid, A. Godt, G. Jeschke, Suppression of ghost distances in multiple-spin double electron-electron resonance, Phys Chem Chem Phys 15(16) (2013) 5854-66.
[27] M.S. Gunnar Jeschke, Miriam Schulteb and Adelheid Godt, Three-spin correlations in double electron–electron resonance, Phys Chem Chem Phys 11(31) (2009) 6580-6591.
[28] K.A. Silvia Valera, Christos Pilotas, Hexian Huang, James H. Naismith, Bela E. Bode, Accurate Extraction of Nanometer Distances in Multimers by Pulse EPR, ChemPubSoc Europe 22 4700 - 4703.
[29] K. Ackermann, B.E. Bode, Pulse EPR distance measurements to study multimers and multimerisation, Molecular Physics 116(12) (2018) 1513-1521.
[30] D.T. Edwards, T. Huber, S. Hussain, K.M. Stone, M. Kinnebrew, I. Kaminker, E. Matalon, M.S. Sherwin, D. Goldfarb, S. Han, Determining the oligomeric structure of proteorhodopsin by Gd3+ -based pulsed dipolar spectroscopy of multiple distances, Structure 22(11) (2014) 1677-86.

[31] V.C. G. Jeschke, P. Ionita, A. Godt, H. Zimmermann, J. Banham, C. R. Timmel, D. Hilger, and H. Jung, DeerAnalysis2006 - a Comprehensive Software Package for Analyzing Pulsed ELDOR Data, Applied Magnetic Resonance 30 (2006) 473 - 498.
[32] S. Ghosh, M.J. Lawless, H.J. Brubaker, K. Singewald, M.R. Kurpiewski, L. Jen-Jacobson, S. Saxena, Cu2+-based distance measurements by pulsed EPR provide distance constraints for DNA backbone conformations in solution, Nucleic Acids Res 48(9) (2020) e49.
[33] D.M. Engelhard, A. Meyer, A. Berndhauser, O. Schiemann, G.H. Clever, Di-copper(ii) DNA G-quadruplexes as EPR distance rulers, Chem Commun (Camb) 54(54) (2018) 7455-7458.
[34] J.E. Lovett, A.M. Bowen, C.R. Timmel, M.W. Jones, J.R. Dilworth, D. Caprotti, S.G. Bell, L.L. Wong, J. Harmer, Structural information from orientationally selective DEER spectroscopy, Phys Chem Chem Phys 11(31) (2009) 6840-8.
[35] A. Meyer, J.J. Jassoy, S. Spicher, A. Berndhäuser, O. Schiemann, Performance of PELDOR, RIDME, SIFTER, and DQC in measuring distances in trityl based bi- and triradicals: exchange coupling, pseudosecular coupling and multi-spin effects, Physical Chemistry Chemical Physics 20(20) (2018) 13858-13869.
[36] K. Ackermann, C. Pliotas, S. Valera, J.H. Naismith, B.E. Bode, Sparse Labeling PELDOR Spectroscopy on Multimeric Mechanosensitive Membrane Channels, Biophysical Journal 113(9) (2017) 1968-1978.
[37] A. Meyer, D. Abdullin, G. Schnakenburg, O. Schiemann, Single and double nitroxide labeled bis(terpyridine)-copper(II): influence of orientation selectivity and multispin effects on PELDOR and RIDME, Phys Chem Chem Phys 18(13) (2016) 9262-71.
[38] L. Fabregas-Ibanez, V. Mertens, I. Ritsch, T. von Hagens, S. Stoll, G. Jeschke, Dipolar pathways in multi-spin and multi-dimensional dipolar EPR spectroscopy, Phys Chem Chem Phys 24(37) (2022) 22645-22660.
[39] A. Giannoulis, R. Ward, E. Branigan, J.H. Naismith, B.E. Bode, PELDOR in rotationally symmetric homo-oligomers, Mol Phys 111(18-19) (2013) 2845-2854.
[40] A.M. Bowen, M.W. Jones, J.E. Lovett, T.G. Gaule, M.J. McPherson, J.R. Dilworth, C.R. Timmel, J.R. Harmer, Exploiting orientation-selective DEER: determining molecular structure in systems containing Cu(ii) centres, Physical Chemistry Chemical Physics 18(8) (2016) 5981-5994.
[41] B.E. Bode, J. Plackmeyer, T.F. Prisner, O. Schiemann, PELDOR Measurements on a Nitroxide-Labeled Cu(II) Porphyrin: Orientation Selection, Spin-Density Distribution, and Conformational Flexibility, The Journal of Physical Chemistry A 112(23) (2008) 5064-5073.
[42] T.F. Prisner, A. Marko, S.T. Sigurdsson, Conformational dynamics of nucleic acid molecules studied by PELDOR spectroscopy with rigid spin labels, Journal of Magnetic Resonance 252 (2015) 187-198.
[43] A.M. Bowen, C.E. Tait, C.R. Timmel, J.R. Harmer, Orientation-Selective DEER Using Rigid Spin Labels, Cofactors, Metals, and Clusters, in: C.R. Timmel, J.R. Harmer (Eds.), Structural Information from Spin-Labels and Intrinsic Paramagnetic Centres in the Biosciences, Springer Berlin Heidelberg, Berlin, Heidelberg, 2013, pp. 283-327.
[44] J. Keeley, T. Choudhury, L. Galazzo, E. Bordignon, A. Feintuch, D. Goldfarb, H. Russell, M.J. Taylor, J.E. Lovett, A. Eggeling, L. Fábregas Ibáñez, K. Keller, M. Yulikov, G. Jeschke, I.

Kuprov, Neural networks in pulsed dipolar spectroscopy: A practical guide, Journal of Magnetic Resonance 338 (2022) 107186.
[45] S.G. Worswick, J.A. Spencer, G. Jeschke, I. Kuprov, Deep neural network processing of DEER data, Science Advances 4(8) eaat5218.

.